HUMAN AIRWAY ORGANOIDS AS A VERSATILE MODEL TO STUDY BSL-4 VIRUS REPLICATION AND PATHOGENESIS

Joo-Hee Wälzlein[1+], Sebastian Reusch[2+], Jenny Ospina-Garcia[1,2], Ruth Olmer[3], Marc A. Schneider[4,5], Christian Klotz[2] and Susann Kummer[1*]

[1] Centre for Biological Threats and Special Pathogens (High containment laboratory), Robert Koch-Institute, Berlin, Germany

[2] Unit "Mycotic and parasitic agents and mycobacteria", Robert Koch-Institute, Berlin, Germany

[3] Leibniz Research Laboratories for Biotechnology and Artificial Organs (LEBAO), Department of Cardiothoracic, Transplantation and Vascular Surgery (HTTG), Biomedical Research in Endstage and Obstructive Lung Disease Hannover (BREATH), German Center for Lung Research (DZL), Hannover Medical School, Hannover, Germany

[4] Translational Research Unit, Thoraxklinik at Heidelberg University Hospital, Heidelberg, Germany

[5] Translational Lung Research Center Heidelberg (TRLC), Member of the German Center for Lung Research (DZL)

* Correspondence author: S.K. (KummerS@rki.de)

+ Equally contributed

No conflict of interest is declared.

Key words: BSL-4 viruses, airway organoids, human infection model

Word count: 1741

Abstract

Research with BSL-4 viruses such as Ebola, Marburg, and Nipah presents significant challenges due to their high virulence and the stringent containment measures required. A major limitation in studying viral pathogenesis and developing therapeutic strategies is the absence of suitable animal models that accurately replicate human disease. In this context, 3D cell culture systems offer significant advantages over traditional 2D monolayer cultures, mimicking native physiological conditions including cell polarization and composition. Human airway organoids, derived from pluripotent or adult stem cells, closely replicate the structure and function of the human respiratory system, providing a relevant and accessible environment for studying viral replication and pathogenesis. In contrast to conventional cell lines, airway organoids enable investigation of virus-host interactions within a human tissue context, providing insights that are more directly translatable to human disease. In our study, we generated airway organoids from both clinical donor tissues and commercially available nasal epithelial cells and showed in comparative analyses with whole lung tissue that these organoids are comparable in terms of cell composition. Despite donor-specific variations due to genetic factors, airway organoids derived from different sources and donors exhibit a remarkably similar cellular make-up. We further demonstrated that organoids derived from nasal swabs can effectively replicate BSL-4 viruses, establishing them as a standardized 3D model for broader research applications and advancing our understanding of these pathogens, especially in the absence of reliable animal models.

Author Summary

This study establishes human airway organoids as a robust model for investigating BSL-4 pathogens, such as Ebola, Marburg, and Nipah virus. Airway organoids represent reliable systems due to their ability to replicate the complexity of human respiratory epithelia and support viral infection. These organoids exhibit high susceptibility to these viruses, allowing for subsequent analysis of infection kinetics, immune evasion, and tissue-specific tropism within a controlled environment. This platform provides a powerful tool for antiviral testing and studying virus-host interactions, thus helping bridge critical gaps in high-containment virus research.

Introduction

A significant challenge in studying BSL-4 viruses, such as Ebola, Marburg, and Nipah, is the absence of animal models that accurately replicate the disease progression observed in humans. This limitation hinders our ability to fully understand their pathogenesis and develop effective therapies for these highly virulent pathogens. Ebola virus causes severe hemorrhagic fever with high mortality rates, primarily in sub-Saharan Africa. It spreads through direct contact with body fluids and can lead to widespread outbreaks, as seen during the 2014-2016 epidemic in West Africa (Ebola Situation Report

30th March, 2016)). Marburg virus, a close relative of Ebola, also causes hemorrhagic fever with similar transmission and clinical outcomes. Both viruses belong to the Filoviridae family and are known for their rapid disease progression and high case fatality rates [1]. In contrast, Nipah virus, a member of the Paramyxoviridae family, causes encephalitis and respiratory illness. First identified in Malaysia in 1998, Nipah virus has since caused multiple outbreaks across South and Southeast Asia [2-5]. These zoonotic viruses are typically transmitted to humans from animals such as fruit bats or pigs. Currently, there are no specific treatments or vaccines available (with exception of the Ebola vaccine, which is only effective against the Ebola Zaire strain) [6-8].

Given the lack of suitable animal models, human stem cell-derived organoids offer a promising alternative for studying these viruses in a controlled environment that closely mimics human tissue [9]. This approach not only allows for the examination of virus-host interactions, but also facilitates the testing of potential therapeutic interventions, providing insights that are more predictive of human outcomes. To provide proof-of-concept, we compared several epithelial organoids derived from respiratory tissue to evaluate cell type conformity using standardized culture protocols and demonstrate the utility of these cultures for studying BSL-4 viruses in a Biosafety Level 4 environment.

Organoids are three-dimensional, self-organizing structures derived from stem cells that better replicate organ physiology compared to 2D or conventional 3D cell cultures using immortalized cell lines [10, 11]. While pluripotent stem cell-derived organoids mimic organogenesis, providing high-fidelity models of pathophysiological complexity in organ development, adult stem cell-derived organoids retain organ identity and genetic stability over time [1, 12]. Culture protocols for adult stem cell derived organoids are relatively straightforward and can easily be established in conventional cell culture laboratories. Moreover, transcriptomic studies show that adult stem cell-derived organoids exhibit gene expression profiles closely resembling their tissue of origin, particularly for airway organoids, which closely align with primary lung tissue profiles [13, 14]. This tissue-specific similarity makes them valuable models for studying organ-specific pathologies.

Results

Airway organoids from various source material, from donor 1, 2 (both healthy lung tissue) and HNEpCs (commercial nasal epithelial cells) exhibited similar morphology and cellular marker expression typical of human respiratory epithelial tissue (**Fig 1**). Cystic and solid structures were observed, with cystic formations, mostly larger than solid structures, characterized by cavities filled with mucus or cell debris becoming larger over time (**Fig 1A-C**). Nasal epithelial cell-derived organoids predominantly formed smaller, solid structures, with some cystic formations appearing in long-term cultures (**Fig 1C**). Immunofluorescence (IFA) and qPCR analysis confirmed the presence and localization of basal cells

(keratin 5, KRT5), goblet cells (mucin 5AC, MUC5AC), ciliated cells (acetylated tubulin, AcTUB), and club cells (secretoglobin family 1A member 1, SCGB1A1) in all organoids, consistent with primary airway tissue (**Fig 1D-E**; **Fig 2** [15]). Specifically, IFA of donor 2 and HNEpC-derived organoids revealed comparable staining for all markers. Comprehensive qPCR analysis verified the expression of all major airway epithelial cell types, with levels generally comparable to or exceeding those observed in lung tissue (**Fig 2**). Although some single marker genes showed significant donor-related variation, a notable difference between nasal and lung-derived organoids was observed in markers for ciliated cells (*FOXJ1, SNTN*). This was expected as ciliated cells are more abundant in nasal epithelial tissue in comparison to lower airway epithelia [16]. Overall, the analysis demonstrated that airway organoids derived from different sources exhibit consistent cellular characteristics and mimic human airway tissue effectively. Although nasal organoids displayed smaller lumens and a higher proportion of ciliated cells compared to lung-derived organoids, they showed stable comparable cellular composition.

Figure 1: **Microscopic analysis of human airway organoids (AOs) focusing on their morphology and the spatial localisation of cellular marker proteins. A-C**: Bright-field images of AOs at different days of cultivation as indicated. Scale bars = 50 µm. Images were taken employing a widefield microscope and a 20x air objective (d = day). **D/E**: Immunofluorescence staining of AOs derived from adult stem cells of human lung tissue from donor 2 or HNEpC using antibodies specific to keratin5 (KRT5), mucin5AC (Muc5AC), acetylated tubulin (AcTub), and uteroglobin (SCGB1A1). Cell nuclei were counterstained with DAPI and F-actin with phalloidin, respectively. Image acquisition was performed using a confocal laser scanning microscope and a 20x immersion oil objective. Scale bars = 100 µm.

Figure 2: qPCR-analysis of human airway organoids (AOs) reveals expression of all major airway epithelial marker genes comparable to human lung tissue. Boxplots show the median and interquartile range, whiskers represent the highest and lowest values, outliers are plotted as dots. D1 = donor 1, D2 = donor 2, HNEpC = human nasal epithelial cells. Statistical significance was calculated using one-way ANOVA, followed by a post-hoc Tukey`s test (ns = $p > 0.05$; * = $p \leq 0.05$; ** = $p \leq 0.01$; *** = $p \leq 0.001$; **** = $p \leq 0.0001$).

Next, we used nasal organoids for infection studies with BSL-4 viruses. Despite their representation of smaller airways and higher abundance of ciliated cells compared to bronchial organoids, this choice was driven by their commercial availability and therefore easy accessibility. Strikingly, the nasal-derived organoids showed high susceptibility to Marburg (MARV), Nipah (NiV), and Ebola Zaire virus (EBOV). These results mark the first proof-of-concept for using these respiratory organoids to study high-risk pathogens in a controlled environment. Viral replication and release were monitored by quantifying the viral genome equivalents present within the organoids (**Fig 3**). Following incubation with the initial virus input, a notable increase in viral genome equivalents was detected, indicating effective viral replication

within the nasal-derived organoids. We further investigated the presence of putative entry markers, namely Niemann-Pick disease, type C1 (NPC1) for Ebola [17] and Marburg virus and Ephrin B2 and B3 (EFNB2, EFNB3) for Nipah virus [18, 19], by qPCR analysis. Transcripts of these proteins were detected at significant levels (data not shown), leading the way to future functional studies.

Figure 3: **HNEpC-derived airway organoids (AOs) exhibit viral replication following infection with Ebola (EBOV), Marburg (MARV), and Nipah (NiV) virus.** AOs were infected with EBOV, MARV and NiV. At 3 days post infection virus-specific copies per mL were quantified by qRT-PCR. Controls (ctrl) were exposed to the viruses for 5 min only. Statistical significance was calculated using unpaired t-test (* = $p \leq 0.05$; ** = $p \leq 0.01$).

Discussion

In this study, we demonstrated that airway organoids from different origin exhibit remarkable consistency in cell type composition, yet maintain regional-specific tissue characteristics. These models are highly susceptible to infection and replication of BSL-4 viruses. By providing insights into tissue-specific tropism and viral entry mechanisms, they may help uncover the molecular determinants that enable viruses like Marburg, Nipah or Ebola virus (MARV, NiV, EBOV) to selectively infect certain tissues, such as the respiratory tract in future studies. Additionally, when supplemented with immune cells, airway organoids allow real-time analysis of immune dynamics, making them well-suited models to study immune evasion strategies of these viruses [20]. Moreover, they also represent a valuable model to study vascular endothelial interactions, helping to clarify how hemorrhagic viruses disrupt blood-tissue barriers and contribute to vascular pathology.

For therapeutic applications, airway organoids provide a robust platform to screen antiviral agents and evaluate tissue-specific drug efficacy and toxicity, with potential implications for precision medicine [21, 22]. Finally, these models facilitate exploration of virus-host interactions and virus-induced metabolic shifts, which could identify novel therapeutic targets.

The three-dimensional architecture of organoids provides an improved representation of host-virus interactions at cellular and molecular levels compared to conventional 2D cell culture systems. In the absence of suitable animal models, organoids allow for physiologically relevant analysis of BSL-4 pathogens, enhancing our understanding of complex viral behaviour and therapeutic responses. Future research should focus on refining culture protocols and enhancing physiological relevance of organoids through improved vascularization, blood perfusion, and immune cell integration.

In conclusion, our proof-of-concept study provides an easy to adapt method to study BSL-4 viruses in an advanced organoid-based airway cell culture model using commercially available cells and published, robust culture protocols.

Material and Methods

Patient samples. Patient-derived lung cells were provided by Lung Biobank Heidelberg, a member of the BioMaterialBank Heidelberg (BMBH) and the platform biobanking of the German Center for Lung Research (DZL). All patients signed an informed consent and study was approved by the ethics committees of Heidelberg and Berlin (S-270/2001 (biobank vote) and EA2/090/20 (study vote).

Organoid Culture and Maintenance. Organoid cultures were established from cryopreserved lung biopsy cells following protocols from Zhou and Sachs [1,3]. Briefly, cells were thawed into DMEM/Ham F-12 medium with ROCK inhibitor, centrifuged, and seeded in organoid medium into T25 flasks. Cells were later transferred into 6-well plates with Cultrex BME for 3D culturing, and medium was replaced weekly. For passaging, cells were enzymatically dissociated with TrypLE, centrifuged, and re-embedded in Cultrex BME (see Supplement for details on culture medium and methods).

Viruses and Infection. BSL-4 viruses, including Ebola-GFP, Ebola, Marburg, and Nipah, were obtained and titrated following standard protocols. Organoids derived from nasal epithelial cells were cultured and infected following protocols detailed in the Supplement. Infections were performed at BSL-4 containment.

RNA Purification, cDNA Synthesis, and qPCR. Organoid RNA was extracted using the Zymo Quick-RNA Kit and converted to cDNA with the High Capacity RNA-to-cDNA Kit. qPCR was performed using both one- and two-step protocols to quantify viral RNA and analyse gene expression abundance. Primer sequences and detailed qPCR protocols are available in the Supplement.

Immunofluorescence Staining and Microscopy. Organoids were fixed, permeabilized, and stained using primary and secondary antibodies to detect relevant markers. Image acquisition was performed on a Leica STELLARIS 8 microscope, and images were processed with ImageJ. Full antibody list and staining procedures can be found in the Supplement.

Acknowledgments

We thank Andreas Kurth for kindly providing the possibility to perform the BSL-4 experiments using the BSL-4 containment lab at the Centre for Biological Threats and Special Pathogens, Robert Koch-Institute, Berlin, Germany. We thank Carmen Hoppstock, Nicole Kromarek, Elke Radam and Gudrun Kliem for excellent technical support.

Funding

Marc A. Schneider and Carmen Hoppstock were partly funded by the German Center for Lung Research (DZL, 82DZL00402). All other work was funded by Robert Koch-Institute.

Author contributions

Conceptualization:	Susann Kummer, Christian Klotz, Sebastian Reusch, Joo-Hee Wälzlein
Formal analysis:	Joo-Hee Wälzlein, Sebastian Reusch, Jenny Ospina-Garcia, Christian Klotz, Susann Kummer
Investigation:	Jenny Ospina-Garcia, Sebastian Reusch, Joo-Hee Wälzlein
Methodology:	Sebastian Reusch, Joo-Hee Wälzlein, Christian Klotz, Susann Kummer
Project administration:	Christian Klotz, Susann Kummer
Resources:	Marc A. Schneider, Ruth Olmer, Christian Klotz, Susann Kummer
Supervision:	Susann Kummer, Christian Klotz
Visualization:	Sebastian Reusch, Jenny Ospina-Garcia, Joo-Hee Wälzlein
Writing – original draft:	Susann Kummer, Christian Klotz, Joo-Hee Wälzlein, Sebastian Reusch
Writing – review & editing:	Susann Kummer, Christian Klotz, Joo-Hee Wälzlein, Sebastian Reusch, Jenny Ospina-Garcia, Marc A. Schneider, Ruth Olmer

References

1. Hofer, M. and M.P. Lutolf, *Engineering organoids.* Nat Rev Mater, 2021. **6**(5): p. 402-420.
2. Chua, K.B., et al., *Nipah virus: a recently emergent deadly paramyxovirus.* Science, 2000. **288**(5470): p. 1432-5.
3. Hsu, V.P., et al., *Nipah virus encephalitis reemergence, Bangladesh.* Emerg Infect Dis, 2004. **10**(12): p. 2082-7.
4. Kulkarni, D.D., et al., *Nipah virus infection: current scenario.* Indian J Virol, 2013. **24**(3): p. 398-408.
5. Sharma, V., et al., *Emerging trends of Nipah virus: A review.* Rev Med Virol, 2019. **29**(1): p. e2010.
6. Edgar, S., et al., *Effects of collagen-derived bioactive peptides and natural antioxidant compounds on proliferation and matrix protein synthesis by cultured normal human dermal fibroblasts.* Sci Rep, 2018. **8**(1): p. 10474.
7. Mishra, G., V. Prajapat, and D. Nayak, *Advancements in Nipah virus treatment: Analysis of current progress in vaccines, antivirals, and therapeutics.* Immunology, 2024. **171**(2): p. 155-169.
8. Groseth, A., H. Feldmann, and J.E. Strong, *The ecology of Ebola virus.* Trends Microbiol, 2007. **15**(9): p. 408-16.
9. Aguilar, C., et al., *Organoids as host models for infection biology - a review of methods.* Exp Mol Med, 2021. **53**(10): p. 1471-1482.
10. Sachs, N., et al., *Long-term expanding human airway organoids for disease modeling.* EMBO J, 2019. **38**(4).
11. Clevers, H., *Modeling Development and Disease with Organoids.* Cell, 2016. **165**(7): p. 1586-1597.
12. Novelli, G., et al., *Organoid factory: The recent role of the human induced pluripotent stem cells (hiPSCs) in precision medicine.* Front Cell Dev Biol, 2022. **10**: p. 1059579.

13. Huch, M. and B.K. Koo, *Modeling mouse and human development using organoid cultures.* Development, 2015. **142**(18): p. 3113-25.
14. Drost, J. and H. Clevers, *Organoids in cancer research.* Nat Rev Cancer, 2018. **18**(7): p. 407-418.
15. Salgueiro, L., et al., *Generation of Human Lung Organoid Cultures from Healthy and Tumor Tissue to Study Infectious Diseases.* J Virol, 2022. **96**(7): p. e0009822.
16. Rogers, T.D., et al., *Regional Differences in Mucociliary Clearance in the Upper and Lower Airways.* Front Physiol, 2022. **13**: p. 842592.
17. Igarashi, M., T. Hirokawa, and A. Takada, *Structural and Energetic Basis for Differential Binding of Ebola and Marburg Virus Glycoproteins to a Bat-Derived Niemann-Pick C1 Protein.* J Infect Dis, 2023. **228**(Suppl 7): p. S479-S487.
18. Bowden, T.A., et al., *Structural basis of Nipah and Hendra virus attachment to their cell-surface receptor ephrin-B2.* Nat Struct Mol Biol, 2008. **15**(6): p. 567-72.
19. Xu, K., et al., *Host cell recognition by the henipaviruses: crystal structures of the Nipah G attachment glycoprotein and its complex with ephrin-B3.* Proc Natl Acad Sci U S A, 2008. **105**(29): p. 9953-8.
20. Baseler, L., et al., *The Pathogenesis of Ebola Virus Disease.* Annu Rev Pathol, 2017. **12**: p. 387-418.
21. Li, H., et al., *Applications of lung cancer organoids in precision medicine: from bench to bedside.* Cell Commun Signal, 2023. **21**(1): p. 350.
22. Vazquez-Armendariz, A.I. and P.R. Tata, *Recent advances in lung organoid development and applications in disease modeling.* J Clin Invest, 2023. **133**(22).
23. Zhou, J., et al., *Differentiated human airway organoids to assess infectivity of emerging influenza virus.* Proc Natl Acad Sci U S A, 2018. **115**(26): p. 6822-6827.
24. Volchkov, V.E., et al., *Recovery of infectious Ebola virus from complementary DNA: RNA editing of the GP gene and viral cytotoxicity.* Science, 2001. **291**(5510): p. 1965-9.
25. Kärber, G., *Beitrag zur kollektiven Behandlung pharmakologischer Reihenversuche.* Archiv f. experiment. Pathol. u. Pharmakol 1931. **162**: p. 480–483.
26. Bustin, S.A., et al., *The MIQE guidelines: minimum information for publication of quantitative real-time PCR experiments.* Clin Chem, 2009. **55**(4): p. 611-22.

SUPPLEMENT

Material and Methods

Organoid cultures and maintenance

Organoid cultures are based on established protocols outlined by Zhou and Sachs [10, 23]. Cryopreserved cells of lung biopsies containing adult stem cells (see Table 1), preserved in a 10% DMSO solution, were thawed in a 37°C water bath. Subsequently, these cells were resuspended in (a 15 mL Falcon tube containing) 5 mL of pre-warmed DMEM/Ham F-12-Gibco medium (Gibco™ CAT#12634010), supplemented with 1:1,000 Y-27632 (ROCK inhibitor; AbMole Bioscience CAT#M1817). Following centrifugation at 500 x RCF for 5 min at 4°C, the pellet was resuspended in 10 mL of organoid medium (see Table 2) and seeded in a T25 flask. Cells were incubated overnight at 37°C with 5% CO_2. For subsequent steps of the 3D-culture, all components were kept on ice. The following day, cells from the T25 flask were collected, adherent cells were gently detached using a cell scraper, and transferred to a 15 mL Falcon tube coated with 0.1% BSA, kept on ice. Cells were then centrifuged at 500 x RCF for 5 min at 4°C and the pellet was resuspended in an ice-cold mixture of 70% Cultrex Basement Membrane Extracts (BME, growth factor-reduced Type 2 basement membrane extract; R&D Systems CAT#3533-005-02) and 30% organoid medium. The cells were seeded as 70 µL BME droplet domes in 6-well plates, with each well containing three domes, and a total of one to three wells used, depending on the initial cell number. The plates were incubated for 30 min at 37°C to allow solidification of the BME. Once solidified, 2mL organoid medium was added to the domes and medium was changed twice a week. For subsequent passages and culture expansion, BME droplets were mechanically disrupted by washing over them with organoid medium using a P1,000 tip and then centrifuged at 500 x RCF for 5 min at 4°C. This was followed by enzymatic digestion using TrypLE Express (Gibco™ CAT#12605010), supplemented with 10 µM ROCK inhibitor for 4-8 min at 37°C. Cells were dispersed into a single-cell solution using a blunt needle (18G), followed by the addition of DMEM/Ham F-12 medium supplemented with ROCK inhibitor. After centrifugation as described earlier, cells were embedded again in 70% BME split in a 1:3 or 1:6 ratio, again in the form of droplets

(each well containing three droplets). The organoids used for both characterization and infection experiments underwent two passages after thawing the cells. For each biological sample, a complete 6-well plate was utilized, comprising a total of 18 droplets.

Table 1: Sources of adult stem cells used for airway organoid generation

Material	Source	Description
Donor 1	Lung Biobank Heidelberg, member of the accredited Tissue Bank of the National Center for Tumor Diseases (NCT) Heidelberg, the Biomaterial Bank Heidelberg, and the Biobank platform of the German Center for Lung Research (DZL)	Lung biopsy of non-cancerous tissue from a 70-year-old, non-smoking patient diagnosed with pulmonary carcinoid
Donor 2	Leibniz Research Laboratories for Biotechnology and Artificial Organs (LEBAO), Biomedical Research in Endstage and Obstructive Lung Disease Hannover (BREATH), German Center for Lung Research (DZL), Department of Cardiothoracic, Transplantation and Vascular Surgery Hannover Medical School, Hannover, Germany)	Lung biopsy of non-cancerous tissue from a 50-year-old patient diagnosed with fibrosis
HNEpC	PromoCell (CAT #C-12620, Lot 475Z023)	Primary human nasal epithelial cells isolated from normal human nasal mucosa
Lung tissue	DZL Heidelberg	

Table 2: Complete organoid medium

Medium supplement	Final concentration
Advanced DMEM/F12	1x
R-Spondin 1	500 ng/mL
FGF-7	25ng/mL
FGF-10	100ng/mL
Noggin	100ng/mL
A83-01	500nmol/L
Y-27632	5µmol/L
SB202190	500nmol/L
N-Acetylcysteine	1.25mmol/L
Nicotinamide	5mmol/L
B27	1x
Pen/Strep/Glutamine	100U/mL; 100µg/mL; 1x
Hepes	10mmol/L
Primocin	50µg/mL

Viruses and infection

Ebola-GFP [24], Ebola virus (Makona), and Marburg virus (Musoke) were kindly provided by Prof. Dr. Stephan Becker, Institute for Virology, Philipps-University Marburg, Germany, and Nipah virus (Malaysia) was kindly provided by Heinz Feldmann, Rocky Mountain Laboratory, Hamilton, Montana, USA. All viruses were propagated in green monkey kidney epithelial Vero E6 cells (American Type Culture Collection, Manassas, VA, CAT#CCL-1586). The viral titer was determined using the Spearman and Kärber method, specifically the $TCID_{50}$/mL (Tissue Culture Infectious Dose 50 per milliliter) assay [25].

The experiments involving risk group 4 viruses were conducted at the BSL-4 facility of the Robert Koch-Institute in Berlin, Germany, strictly following standard operating protocols for handling infectious agents. Organoids derived from commercially available airway epithelial cells sourced from nasal swabs were cultured for approximately 20 d prior to infection as previously described. Organoids grown in 18 x 70 µL domes were collected into 15 mL tubes and centrifuged at 500 × RCF for 5 min, leaving a liquid pellet containing the organoids. The supernatant was discarded and BME was removed by incubating the pellet in 3 mL cell recovery solution for 45 min at 4°C with resuspension every 15 min, followed by another centrifugation step. Subsequently, 1260 µL of 70% BME, diluted in organoid medium, was mixed with 25 µl EBOV ($TCID_{50}$ = 2.94x 10^7/mL); 18.4 µl MARV ($TCID_{50}$ = 3.98x 10^7/mL) and 11.7 µl NiV ($TCID_{50}$ = 6.3x10^7/mL), respectively, to reach equal levels of infection doses; organoids were resuspended in this mix avoiding bubble formation on ice. This mixture was then seeded as droplets in 6-well LabTeks plates and incubated at 37°C for 30 min. Once solidified, the BME droplets were maintained for the specified durations in a previously reported medium [10]. Controls were treated simultaneously, but infection was stopped after 1 h. Organoids were collected and pelleted as described above in this section and organoids were re-seeded in 70% BME in the absence of viral input.

RNA purification, reverse transcription and qPCR

The primer pairs (see table 3) for the different markers were validated and efficiency of primers was calculated as described [26].

Table 3: Primer used for qRT-PCR

Target	Sequence	Gene ID
KRT5	Fw: CCAAGGTTGATGCACTGATGG Rev: TGTCAGAGACATGCGTCTGC	3852
MUC5AC	Fw: CAGCACAACCCCTGTTTCAAA Rev: GCGCACAGAGGATGACAGT	4586
SCGB1A1	Fw: TCCTCCACCATGAAACTCGC Rev: AGGAGGGTTTCGATGACACG	7356
FOXJ1*	Fw: AGATCCCACCTGGCAGAATTCAA Rev: CCGAGGCACTTTGATGAAGC	2302
SNTN	Fw: TGTATGCACAGTACCCAGGAC Rev: AGCAGTGGTGGCAATAGCTTT	132203
MUC5B	Fw: GCCTACGAGGACTTCAACGTC Rev: CCTTGATGACAACACGGGTGA	727897
ITGA6*	Fw: ATGCACGCGGATCGAGTTT Rev: TTCCTGCTTCGTATTAACATGCT	3655
TMPRSS2*	Fw: CAAGTGCTCCAACTCTGGGAT Rev: AACACACCGATTCTCGTCCTC	7113
ACE2*	Fw: CAAGAGCAAACGGTTGAACAC Rev: CCAGAGCCTCTCATTGTAGTCT	59272
GAPDH*	Fw: CTCCTGTTCGACAGTCAGCC Rev: CCCAATACGACCAAATCCGTTG	2597
ß-Actin*	Fw: CATGTACGTTGCTATCCAGGC Rev: CTCCTTAATGTCACGCACGAT	60
RPS18*	Fw: AGTTCCAGCACATTTTGCGAG Rev: TCATCCTCCGTGAGTTCTCCA	6222
GFP	Fw: GAGCGCACCATCTTCTTCAA Rev: CTGCTTGTCGGCCATGATATAG	25339618
Ebola Zaire, VP30	Fw: ACT CCT ACT AAT CGC CCG TAA G Rev: ATC AGC CGT TGG ATT TGC T	

Target	Sequence	Gene ID
	Probe: CACCCAA+GGACTCGC	
Marburg, NP	Fw: GTCCTCAGCCAGAAACGAGA Rev: ACCGTTACTTCCACAGGTGT Probe: TCACAGAATCGGGTGTCACAGTCGT	
Nipah Malaysia, NP	Fw: GTTCAGGCTAGAGAGGCAAAATTT Rev: CCCCTTCATCGATATCTTGATCA Probe: CTGCAGGAGGTGTGCTCATTGGAGG	

* Sequence taken from PrimerBank, Harvard Medical School.

This study employed two distinct quantitative polymerase chain reaction (qPCR) protocols. The initial protocol, which utilized a two-step qPCR method, was applied for organoid characterization, while a one-step qPCR approach was implemented for the infection experiments. For the two-step qPCR, 18 organoid domes embedded in BME were collected, centrifuged at 500 x RCF for 5 min at 4°C. Subsequently, the pellet was resuspended in 700 µl of Trizol Reagent (Zymo Research CAT#R2050-1-200) and stored at -80°C until further processing. RNA extraction was performed using the Zymo Quick-RNA Microprep Kit (Zymo Research CAT#R1050) following the manufacturer`s instructions. RNA concentration was assessed using Tecan's NanoQuant Plate. Synthesis of cDNA was employed using the High Capacity RNA-to-cDNA kit (Applied Biosystems-Thermo Fisher Scientific CAT#4387406). 20 µL of the reaction mixture were pipetted into ice-cold RNase-free PCR tubes. During the incubation step, the mixture was heated to 70°C for 5 min without the addition of RT Enzyme Mix, facilitating denaturation and allowing for initial annealing. The RT program encompassed 60 min at 37°C, 5 min at 95°C, and a final step at 4°C. After cDNA synthesis, samples were diluted with nuclease-free water to a concentration of 2 ng/µL in preparation for qPCR analysis. Real-time quantification was carried out using 10 ng (5 µL) of cDNA with SYBR Green LUNA Universal qPCR (New England BioLabs CAT#M3003) on a Bio-Rad CFX96 qPCR real-time thermocycler. For the one-step qPCR, 18 embedded organoids were collected, centrifuged at 500 x RCF for 5 min at 4°C. BME was removed by incubating the pellet in 3 mL cell recovery solution for 45 min at 4°C with resuspension every 15 min. Following another centrifugation step the supernatant was removed and organoids were lysed in 300 µL RLT buffer and RNA was isolated following the manufacturer`s instruction (Qiagen CAT# 74104). RNA samples for one-

step qPCR analysis were diluted with nuclease-free water to 2 ng/µL. Real-time quantification was performed using the SYBR Green One-Step RT-qPCR Kit (New England BioLabs CAT#E3005) with 10 ng of RNA on a Bio-Rad CFX96 qPCR Real-Time thermocycler.

Immunofluorescence staining and laser scanning microscopy.

Organoids were collected and centrifuged at 500 x RCF for 5 min at 4°C. Thereafter, in order to prevent organoid damage, centrifugation was avoided and, cells were allowed to settle naturally. The pellet containing organoids and BME were incubated in cell recovery solution (Corning CAT#CLS354253) for 45 min at 4°C to dissolve the extracellular matrix. During the incubation organoids were diligently resuspended every 10 min using a 0.1% BSA-coated pipette tip. After settling, supernatant was aspirated and the pellet was washed with PBS to eliminate any residual supernatant. Subsequently, the organoids were fixed in 4% paraformaldehyde (PFA, ROTH CAT#0335.1) for 45 min at 4°C. During the fixation process, organoids were gently resuspended every 10 min with a BSA-coated pipette tip. Following fixation, two additional PBS washes were performed. The organoids were then incubated in permeabilization buffer (1xTBS, 0.25% TritonX-100, 0.1 M glycine for 20 min) at room temperature. Following settling, the permeabilization buffer was carefully removed and samples were incubated in blocking buffer (1xTBST, 0.02% Triton-X100, 3% BSA, 1% normal goat serum) for 1 h at room temperature. Primary antibodies (see Table 4) were diluted in 900 µl of blocking buffer as indicated. The organoids were incubated overnight with the primary antibodies at 4°C, washed three times with washing buffer (1xTBS-T containing 0.05% Tween and 0.02% Triton-X100) and allowed to settle before removing the supernatant. Afterwards, the organoids were incubated with the secondary antibodies (see Table 4) in blocking buffer, DAPI for nuclear staining, and phalloidin for actin filament staining at room temperature for approximately 2 h. Following staining, three washes with washing buffer, as described above, were carried out, followed by a final wash with Milli-Q water. Finally, the organoids were gently resuspended in approximately six to eight drops of non-hardening mounting medium (Ibidi, CAT#50001) and placed onto microscope slides. During the mounting process, spaces were left

between the slide and the coverslip to prevent organoid compression. These spaces were sealed with nail polish to ensure proper preservation.

Image acquisition was performed using an inverted fluorescence confocal microscope (Leica STELLARIS 8) with a 20x objective. The imaging software employed was LAS X, with image resolution set to 1024 × 1024 pixels, and subsequent image editing was conducted using ImageJ software.

Table 4: Primary and secondary antibodies employed for immunofluorescence staining

Antibody	Company	Order Number	Dilution	Host
		Primary Antibodies		
Anti-CC10-E11	Santa Cruz	sc365992	10ug/ul	Mouse
Anti-Mucin 5AC	Thermo Fisher	MA5-12178	1:100	Mouse
Anti-acetylated tubulin	Sigma Aldrich	T6793	1:100	Mouse
Anti-Cytokeratin 5	Biolegend	905501	1:100	Rabbit
		Secondary Antibodies		
αMouse IgG (H+L)	Thermo Fisher (Alexa Fluor647)	A28181	1:250	Goat
αRabbit IgG (H+L)	Thermo Fisher (Alexa Fluor647)	A27040	1:500	Goat
Phalloidin iFluor	Abcam (iFluor 488)	ab176753	1:1,000	-
DAPI	Abcam	ab228549	1:500	-

Data analysis

The qRT-PCR data were subjected to analysis using the ΔΔCt method [6]. For assessing the expression changes of the gene of interest (GOI), the mean Cq values of the biological replicates for the GOI were initially computed. These Cq values were then normalised against the reference gene ß-Actin. The obtained results from the control (lung tissue) and donor samples were juxtaposed, and ΔΔCq values were computed.

Statistical analysis was performed using Prism9 software (GraphPad). Ordinary one-way ANOVA was employed for qPCR analyses pertaining to organoid characterization, comparing means across more than two populations, assuming normal distribution and equal variance for all tests. Boxplots show the

median and interquartile range, whiskers represent the highest and lowest values, outliers are plotted as dots. For analysis of qPCR data showing viral replication, unpaired t-test was performed. The presented p-values are as follows: ns (not significant) = $p > 0.05$; * = $p \leq 0.05$; ** = $p \leq 0.01$; *** = $p \leq 0.001$; **** = $p \leq 0.0001$.

Figure 1

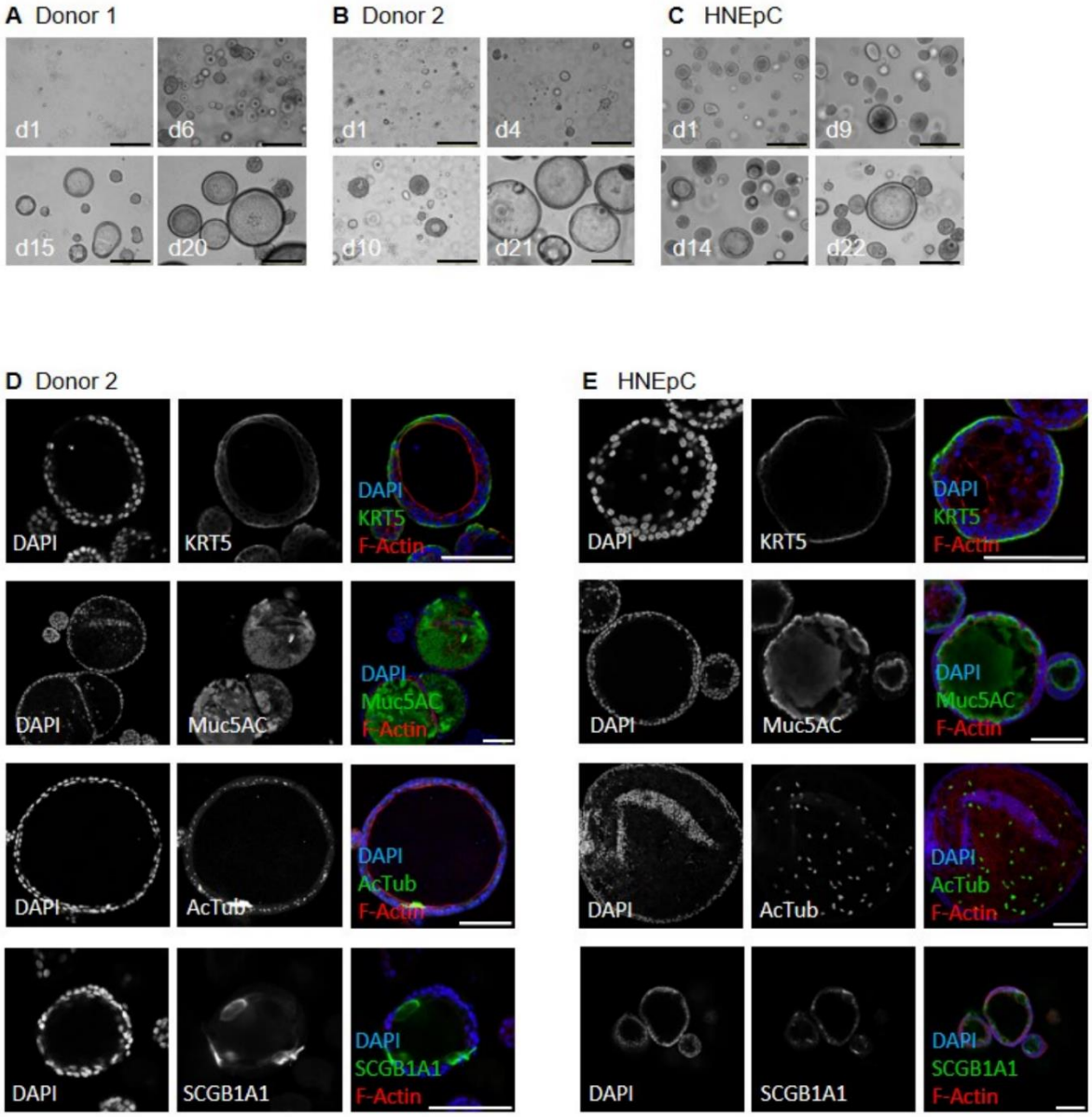
A Donor 1
d1
d6
d15
d20
B Donor 2
d1
d4
d10
d21
C HNEpC
d1
d9
d14
d22
D Donor 2
DAPI
KRT5
DAPI
KRT5
F-Actin
DAPI
Muc5AC
DAPI
Muc5AC
F-Actin
DAPI
AcTub
DAPI
AcTub
F-Actin
DAPI
SCGB1A1
DAPI
SCGB1A1
F-Actin
E HNEpC
DAPI
KRT5
DAPI
KRT5
F-Actin
DAPI
Muc5AC
DAPI
Muc5AC
F-Actin
DAPI
AcTub
DAPI
AcTub
F-Actin
DAPI
SCGB1A1
DAPI
SCGB1A1
F-Actin

Figure 2

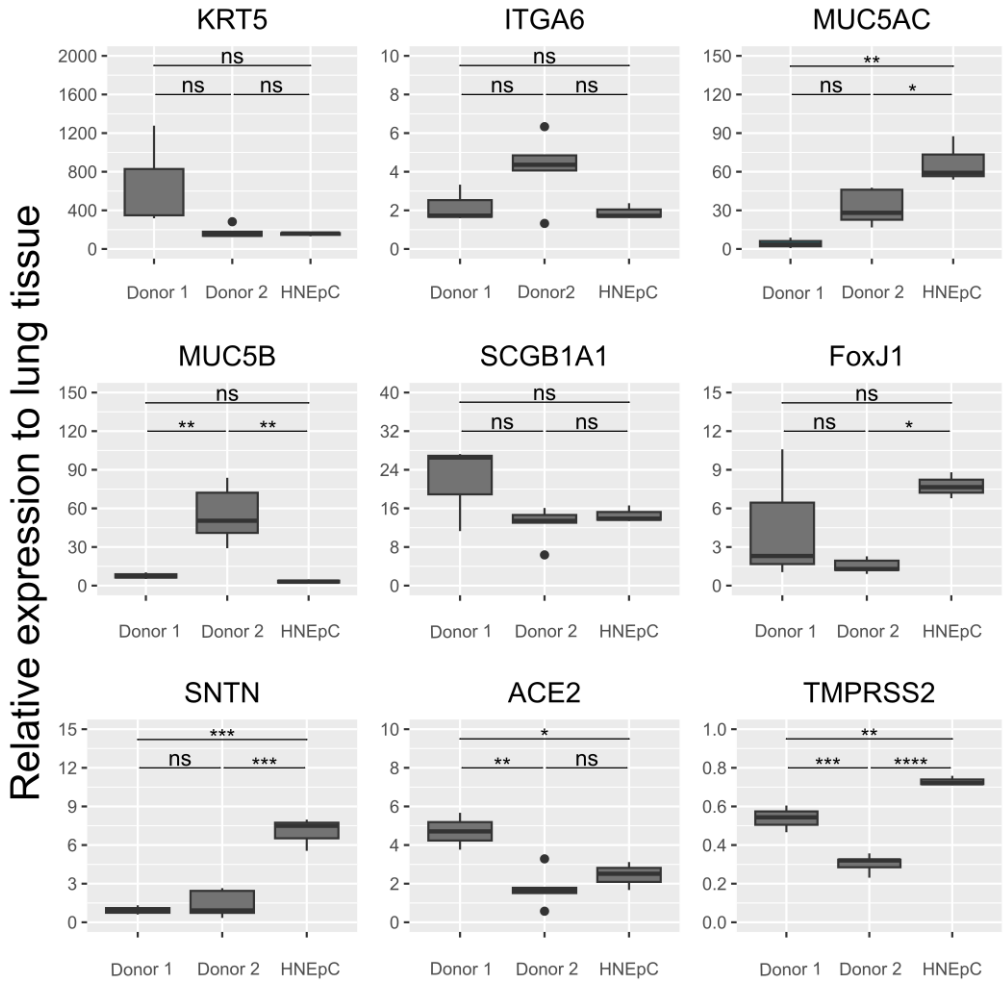
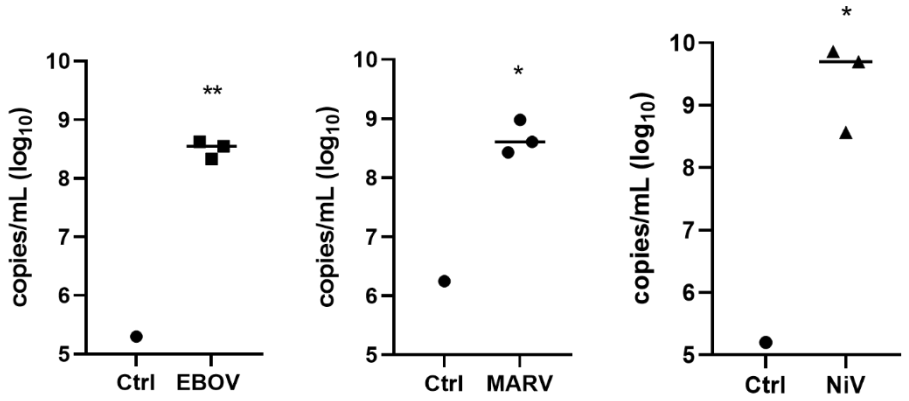
Figure 3